Available online at www.sciencedirect.com

ScienceDirect

IFAC Papers Online CONFERENCE PAPER ARCHIVE

IFAC PapersOnLine 50-1 (2017) 4498–4503

Robust lidar-based closed-loop wake redirection for wind farm control

Steffen Raach * **Sjoerd Boersma** † **Jan-Willem van Wingerden** †
David Schlipf * **Po Wen Cheng** *

* *University of Stuttgart, Germany*
(e-mail: raach@ifb.uni-stuttgart.de).
† *Delft University of Technology, The Netherlands*

Abstract: Wind turbine wake redirection is a promising concept for wind farm control to increase the total power of a wind farm. Further, the concept aims to avoid partial wake overlap on a downwind wind turbine and hence aims to decrease structural loads. Controller for wake redirection need to account for model uncertainties due to the complexity of wake dynamics. Therefore, this work focuses first on modeling a wind farm using an uncertain plant description and second on the design of a robust $\mathcal{H}_\infty$ controller for closed-loop wake redirection by applying standard robust modeling and control techniques on a wind farm. The wake center position is estimated and fed back to a controller which uses the yaw actuator to redirect the wake. For several inflow conditions, step simulations are conducted and system identifications are performed to obtain multiple plant models. This set of models is used to derive a nominal plant and an uncertainty set. Both the nominal model and the uncertainty set define the uncertain plant model. The robust controller is then designed showing promising results in a medium-fidelity CFD simulation model with time-varying inflow conditions.

Keywords: Control of renewable energy, wind energy, wind farm control, wake redirection, robust control, lidar-based control

1. INTRODUCTION

Wind energy is a key technology to meet future renewable energy goals. In past decades, wind energy has developed from a niche to a reliable technology for power production although it has a lower energy per area factor compared to conventional power plants. Pushing this factor to a higher level makes wind energy production more efficient and competitive. In the past, this was mainly done by increasing the wind turbine size. In recent years, clustering wind turbines to a wind farm also increases the efficiency of wind energy power since grid infrastructure is shared. However, by clustering wind turbines, flow interactions between wind turbines play a relevant role. Due to them, a wind turbine in a wake of an other wind turbine produces less power and suffers higher loads due to wake deficit and increased turbulence intensity in the wake. The idea of wind farm control is to take the wake interactions into account while evaluating controllers. Since wake behavior is complex, model errors will most likely occur. This motivates studying the inclusion of uncertainty in the model and evaluate robust controllers for such an uncertain plant.

To increase the total power output of a wind farm, two main wake control concepts have been considered in the last years: axial-induction-based control, and wake redirection control, (see Annoni et al. (2016) and Fleming et al. (2014), respectively). The work in this paper contributes to the field of wake redirection control. See Boersma et al. (2017) for a summary of current wind farm control activities.

Wake redirection has shown promising results in increasing the total power output of an high-fidelity wind farm model, see Gebraad et al. (2016); Fleming et al. (2014). Further, in Raach et al. (2016a), closed-loop wake redirection control increased the power output of an engineering wind farm model even higher. The general idea of wake redirection is to deflect the wake by either yawing the wind turbine or by cyclic blade pitching (see Fleming et al. (2015, 2014)) such that the performance of downwind turbines increases. Having the ability to deflect the wake gives an additional degree of freedom when controlling a wind farm. Partial wake overlaps can be avoided and the total power output can be increased. This motivates the investigation of more reliable solutions for the wake redirection concept and to also include remote sensing devices like lidar.

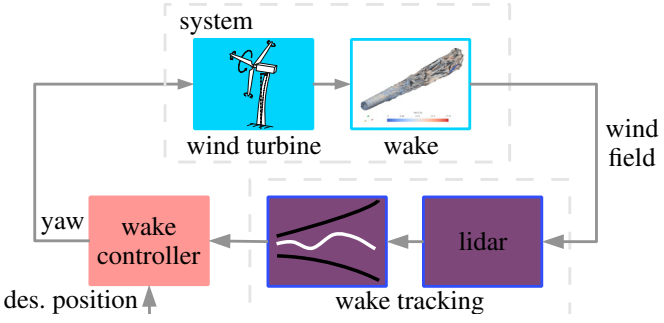

Fig. 1: A block scheme of the general idea of lidar-based closed-loop wake redirection concept.

Lidar-based closed-loop wake redirection was first presented in Raach et al. (2016b,a). In the following, this concept is reviewed and applied on a uncertain plant with which a robust controller is evaluated. The importance of including uncertainty in the model stems from the fact that wake dynamics are complex (nonlinear and time-varying). Hence modeling using

10.1016/j.ifacol.2017.08.380

a set of models (an uncertain plant) instead of only one model will, when correctly choosing the uncertainty set, improve the controller design.

The idea of lidar-based closed-loop wake tracking is to use lidar measurements taken from the wake of the wind turbine and use these to estimate the wake center position. Then, this information is used in a controller which sets the yaw angle of the wind turbine. Altogether, this is done in a closed-loop setting illustrated in Fig. 1. The concept can be divided in an estimation task and a control task, see Raach et al. (2016b). The estimation task deals with processing lidar measurement data to useful information for the controller. Model-based wind field reconstruction techniques are used to obtain the wake position. The controller task deals with providing a controller, which steers the wake to a desired position by using the yaw actuator. This work focuses on the controller task and proposes a robust controller for wake redirection. A nominal $\mathcal{H}_\infty$ controller was designed in Raach et al. (2017). However, if the controller design model deviates from reality due to model mismatches, no performance can be ensured. This further motivates the design of a robust controller. First, model identification is performed to obtain linear models for different atmospheric conditions. These models are then used to obtain a nominal plant and an uncertainty set. Both combined define the uncertain plant. Using this, a robust controller is designed and analyzed with respect to the design criteria. Finally, the control performance is evaluated in a medium-fidelity computational fluid dynamics (CFD) model.

Summarizing, the main contributions of this paper are:

(1) an uncertain plant for lidar-based wake redirection is obtained from simulations of a medium-fidelity CFD model by using identification techniques,
(2) application of robust $\mathcal{H}_\infty$ controller design to lidar-based wake redirection, and
(3) a simulation study with varying atmospheric conditions in a medium-fidelity CFD model with the obtained controller.

This paper is structured as follows: first, the simulation model is briefly reviewed and summarized. Second, the model identification is presented. Third, in Sec. 3 the uncertain model used for controller design is defined. Then, robust controller design is shown in Sec. 4, after which in Sec. 5, simulation results are presented and discussed. In Sec. 6, conclusions are given.

2. SIMULATION MODEL

For this paper, the medium-fidelity CFD wind farm model (WFSim) Boersma et al. (2016) is used. In the following, this model will briefly be described and the wake center estimation approach will be presented.

2.1 Wind farm model WFSim

WFSim is a two-dimensional flow model which can compute flow vectors for a given wind farm topology. The solver is based on the 2D Navier-Stokes equations:

$$\begin{aligned} &\frac{\partial \mathbf{u}}{\partial t} + (\mathbf{u}\cdot\nabla)\mathbf{u} + \frac{1}{\rho}\nabla p - \frac{\mu}{\rho}\nabla^2\mathbf{u} = \mathbf{f}, \\ &\mathbf{u}\cdot\nabla = 0, \end{aligned} \tag{1}$$

$$\text{with } \nabla = [\tfrac{\partial}{\partial x}\ \tfrac{\partial}{\partial y}]^T \text{ and } \nabla^2 = \tfrac{\partial^2}{\partial x^2} + \tfrac{\partial^2}{\partial y^2}. \tag{2}$$

The term $\mathbf{f}$ represents the turbines while $\mathbf{u} = [u\ v]^T$ and p represent the flow velocities and pressure, respectively. The air density ρ and the viscosity μ are considered to be constant. The governing equations are resolved numerically using a spatial and temporal discretization scheme. The discrete state variables u_k, v_k and p_k at time step k are arranged according the grid points, e.g.,

$$u_k = \Big[u_{3,2}\dots u_{3,N_{y-1}}\dots\dots u_{N_{x-1},N_{y-1}}\Big]. \tag{3}$$

The constants N_x and N_y are the number of grid points in the x- and y-direction respectively. Re-writing the obtained set of equations results in the following set of nonlinear algebraic difference equations:

$$\underbrace{\begin{pmatrix} A_x(u_k,v_k) & 0 & B_1 \\ 0 & A_y(u_k,v_k) & B_2 \\ B_1^T & B_2^T & 0 \end{pmatrix}}_{A(x_k)\in\mathbb{R}^{n\times n}} \underbrace{\begin{pmatrix} u_{k+1} \\ v_{k+1} \\ p_{k+1} \end{pmatrix}}_{x_{k+1}} = \underbrace{\begin{pmatrix} b_1(u_k,v_k)+f_k^x(u_k,v_k) \\ b_2(u_k,v_k)+f_k^y(u_k,v_k) \\ b_3 \end{pmatrix}}_{b(x_k)\in\mathbb{R}^{n\times 1}}, \tag{4}$$

with $n = n_u + n_v + n_p$ and $u_k \in \mathbb{R}^{n_u}, v_k \in \mathbb{R}^{n_v}, p_k \in \mathbb{R}^{n_p}$ the velocity vectors in the x-direction, y-direction and the pressure vector at time k, respectively. Each component of u_k, v_k and p_k represents at time k a velocity and pressure respectively at a point in the field defined by the subscript. Computational cost for solving this set of equations is kept low by exploiting sparsity and structure. The terms $b_1(u_k,v_k)$, $b_2(u_k,v_k)$ and b_3 represent the boundary conditions and the terms $f_k^x(u_k,v_k)$ and $f_k^y(u_k,v_k)$ the turbines. Both will be described next.

Boundary and initial conditions For the u_k and v_k velocity, first order conditions are prescribed on one side of the grid related to the ambient inflow defined by u_b and v_b. Zero stress boundary conditions are imposed on the other boundaries. For the initial conditions, all u_k and v_k velocity components in the field are defined as u_b and v_b respectively, the boundary velocity components. The initial pressure field is set to zero.

Turbine model According to momentum theory, the following forcing term can be defined:

$$f_k = C_T(a_k)\frac{1}{2}\rho\,(U_k^\infty)^2\,\Delta x, \tag{5}$$

with thrust coefficient $C_T(a_k)$ depending on the axial induction factor a_k, rotor upwind velocity U_k^∞ and Δx the spatial discretization of the rotor disk. The following expression for $C_T(a_k)$ is proposed in Marshall (2005) and used in WFSim:

$$C_T(a_k) = \begin{cases} 4a_kF(1-a_k), & \text{if } 0 \le a_k \le 0.4 \\ \frac{8}{9} + \frac{36F-40}{9}a_k + \frac{50-36F}{9}a_k^2 & \text{if } 0.4 < a_k < 1 \end{cases} \tag{6}$$

The scaling factor F is set to 1.75. Since U_k^∞ is difficult to measure in a wind farm, it is more realistic to write the force in terms of the rotor velocity. The following relations are defined:

$$\beta = \frac{a_k}{1-a_k}, \quad U_k^\infty = \frac{U_k^r\cos(\gamma_k-\phi_k)}{1-a_k}, \quad U_k^r = \sqrt{\left(u_k^r\right)^2 + \left(v_k^r\right)^2},$$

with U_k^r the flow velocity vector at the rotor with direction defined by the wind direction angle ϕ_k and the yaw angle γ_k of the turbine (see Fig. 2). Substituting these relations in Eq. (5) yields the force expression S_k:

$$f_k = \frac{1}{2}\rho C_T(\beta_k)\left[U_k^r\cos(\gamma_k-\phi_k)(\beta_k+1)\right]^2\Delta x. \tag{7}$$

The forces in the x- and y-direction are now defined as:

$$f_k^x(u_k,v_k) = -f_k\cos(\gamma_k), \qquad f_k^y(u_k,v_k) = f_k\sin(\gamma_k). \tag{8}$$

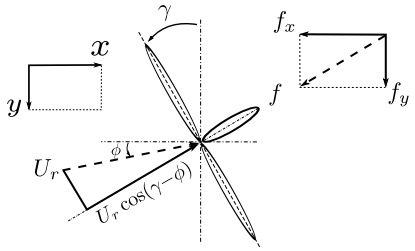

Fig. 2: Schematic representation of a turbine with yaw angle γ_k, wind direction angle at the rotor ϕ_k and rotor velocity U_k^r. Note that in the figure we omit the time index k. Also, the force f_k is determined for each cell in which the rotor is present. Figure taken and adapted from Jiménez et al. (2010).

2.2 Wake tracking in WFSim

In this work, a relatively simple wake center estimation approach is used due to the homogeneous atmospheric conditions. To estimate the wake position, the wind speed profile at a defined measurement distance behind the wind turbine is used (here 2.5 times the rotor diameter). There, the area center point between the two points where the wind speed is first below 93% of the free stream velocity U_k^∞ from each side is computed. The center point is then used as an estimation of the wake position. In the future, when using lidar measurement data to estimate the wake position, more advanced methods like a model-based wake tracking approach is needed (see *e.g.* Raach et al. (2016b)).

3. UNCERTAIN MODEL FOR CONTROLLER DESIGN

In the following, multiple identification procedures are performed on the nonlinear medium-fidelity CFD model described in Sec. 2.1 for different atmospheric conditions. The objective is to obtain an uncertain linear model of the form:

$$G_p(s) = G_0(s)\Big(1 + W(s)\Delta(s)\Big) \quad \text{with } \Delta(s) \in \underline{\Delta} \tag{9}$$

that is required for the robust $\mathcal{H}_\infty$ controller synthesis used in this paper. The input of (9) is the yaw angle and the output is the wake centerline. The procedure is the following: 1) identify several models, 2) calculate a nominal model representative of the identified models, and 3) define the uncertainty set.

3.1 Model identification setup

Step responses are used to estimate system dynamics and obtain a model for each step simulation because they excite specifically those dynamics we want to control. In this work, we conduct simulations for three different wind speeds, 6 m/s, 8 m/s, and 10 m/s, and within each wind speed simulation, five Δ5 deg steps starting from 0 deg to 25 deg are applied by the yaw actuator. The measurements are used in the model identification procedure to estimate the dynamics. To obtain offset free models only the transient behavior in the output is used for model identification.

Altogether, fifteen steps are analyzed and fifteen models are identified. The step simulation results can be seen in Fig. 3. The two main aspects in which they differ are the steady-state amplitude and the dynamical behavior. These differences are due to the changing inflow conditions which change the propagation of the flow. Further, all models show inverse response behavior (non-minimum phase behavior) that limits the achievable closed-loop bandwidth.

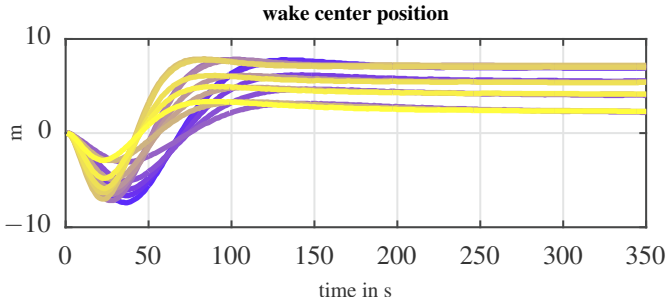

Fig. 3: A comparison of the step response simulation results of three different wind speeds, 6 m/s, 8 m/s, and 10 m/s, and within each wind speed simulation five Δ5 deg steps from 0 deg to 25 deg are applied by the yaw actuator. The wake center is estimated in a downwind distance of 2.5 times the rotor diameter. The steady state is removed to compare the dynamics and the final steady state. The coloring starts at dark blue for the step results at 6 m/s and ends with yellow with the last step response at 10 m/s.

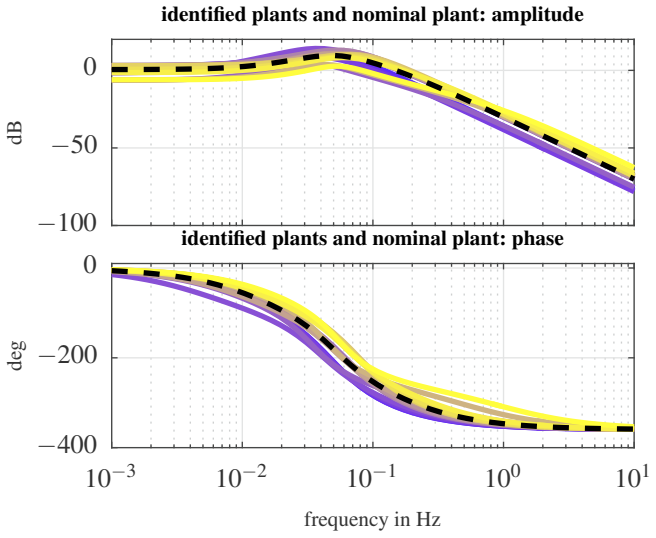

Fig. 4: Bode plot of all identified models $G_l(s)$ and (dashed) the resulting nominal plant $G_0(s)$.

3.2 Model identification

There are several methods to obtain a model from input-output time simulations. Here, a method of the Model Identification Toolbox of Matlab is used to estimate a continuous transfer function with a predefined number of poles, zeros, and a time delay. For more information on the methodology of the model identification see Ljung (1999). The recorded input (yaw angle) and the recorded output (estimated wake center), are used in the model identification.

As mentioned, the number of poles and zeros have to be predefined. For this work, the number of zeros and poles are chosen in a way that the identification results in a normalized root mean squared error of less than 5% between the model and the recorded output. $n_Z = 2$ zero, and $n_P = 5$ poles are set for each identification. This yields a set of models of the form:

$$G_l(s) = \frac{K_l(z_{l1}s+1)(z_{l2}s+1)}{(p_{l1}s+1)(p_{l2}s+1)(p_{l3}s+1)(p_{l4}s+1)(p_{l5}s+1)} \tag{10}$$

with p_{lm} the poles, z_{lm} the zeros, and K_l the static gain of the identified models $G_l(s)$ for $l = \{1,2,\ldots,15\}$. In Fig. 4 the bode plot of all identified models $G_l(s)$ for wind speeds of 6 m/s, 8 m/s, and 10 m/s is presented.

3.3 Uncertainty

The idea of robust control is to ensure stability and performance for a set of models. This set is defined as:

$$G_p(s) = G_0(s)\Big(1 + W(s)\Delta(s)\Big) \tag{11}$$

with the nominal plant $G_0(s)$, a weighting filter $W(s)$, and uncertainty $\Delta(s)$. (11) will be referred to as the uncertain plant. In this paper we have a SISO system assuming to have complex uncertainty hence $\Delta \in \mathbb{C}$ with property $||\Delta(s)||_\infty \leq 1$. In order to define the nominal model $G_0(s)$ we, for each frequency ω_j, first compute:

$$\begin{aligned} |g_0(i\omega_j)| &= \frac{1}{m}\sum_{l=1}^{m} |G_l(i\omega_j)|, \\ \angle g_0(i\omega_j) &= \frac{1}{m}\sum_{l=1}^{m} \angle G_l(i\omega_j), \end{aligned} \tag{12}$$

with $\angle g_0(i\omega_j)$ defined as the average phase of $G_l(s)$ for the frequency ω_j and $|g_0(i\omega)|$ the average amplitude. m is the number of considered models ($m = 15$). The average model for the frequency ω_j is then defined as:

$$g_0(i\omega_j) = |g_0(i\omega_j)|^{i\angle g_0(i\omega_j)}, \tag{13}$$

and the bode plot of it is shown in Fig. 4 compared to the identified models G_l. In order to obtain an equivalent model structure as defined in (10), an identification is performed on $g_0(i\omega_j)$ resulting in the nominal plant $G_0(s)$. Having obtained the nominal plant $G_0(i\omega)$ the uncertainty set can be calculated by evaluating

$$L_l(i\omega_j) = \left|\frac{G_l(i\omega_j) - G_0(i\omega_j)}{G_0(i\omega_j)}\right|, \tag{14}$$

for all l models. The amplitude of the set is plotted in Fig. 5. The weighting filter $W(s)$ determines the uncertainty size and should have the property

$$W(i\omega_j) \geq L_l(i\omega_j). \tag{15}$$

In order to ensure this property, the following expression can be used to define the amplitude of $W(s)$ for the frequency ω_j:

$$|W(i\omega_j)| = \max_l \left|\frac{G_l(i\omega_j) - G_0(i\omega_j)}{G_0(i\omega_j)}\right|, \tag{16}$$

Since we assume $W(s)$ to be without right-half-plane zeros, the uncertainty weight is uniquely defined by its amplitude response given in (16). It is interesting to have a low order weighting filter because this order will, *i.a.*, determine the controller order. Hence the choice of this order is important, we fit a fixed order transfer function on $W(s)$ (6th order). In the following section, a controller will be designed for the uncertain plant.

4. CONTROLLER DESIGN

In the previous section, the uncertain plant G_p has been defined. Note that for the sake of simplicity, we omit, in the remainder of this paper the frequency dependency of the transfer functions. In the remainder of this section, the controller design using the uncertain plant will be presented.

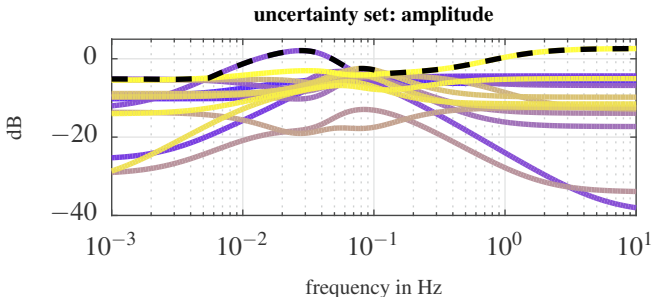

Fig. 5: The uncertainty set calculated by (14) and the resulting weighting filter $W(i\omega)$ (dashed).

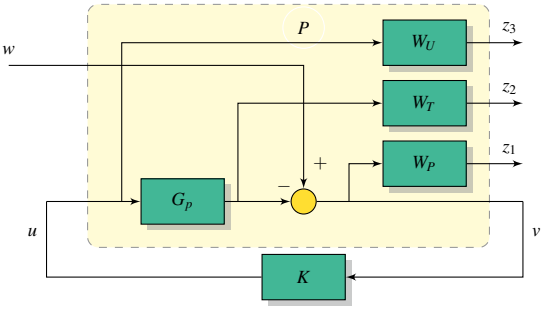

Fig. 6: Generalized plant P with performance signals z_1, z_2, and z_3 and wake center position reference w. Furthermore, we have the identified uncertain model G_p, the performance weights W_P, W_U and W_T, the measured output v (wake center) and controller K with control signal u, the yaw angle.

The robust $\mathcal{H}_\infty$ controller design approach is applied in this paper. By placing and choosing performance weights, closed-loop transfer functions can be shaped and in addition, performance can be ensured for all closed-loop plants in the set assuming nominal stability. It is illustrated in Fig. 6 how the performance weights are placed in the generalized plant P. To find a robust controller K, the following problem is solved:

$$\min_K \ \big|\big|N_p\big|\big|_\infty, \ \text{with} \ N_p = \begin{bmatrix} W_P S_p \\ W_U K S_p \\ W_T T_p \end{bmatrix}. \tag{17}$$

N_p describes the map of the reference position of the wake center, w, to the performance signal, $z = N_p w$. Furthermore, we have

$$S_p = (1 + G_p K)^{-1}, \quad T_p = G_p K S_p, \tag{18}$$

and $N_p = \texttt{lft}(\Delta, N)$ and $N = \texttt{lft}(P, K)$, with the linear fractional transformation `lft`. Robust performance is achieved when $||N||_\infty < 1$ assuming nominal stability for all $||\Delta(s)||_\infty \leq 1$. This definition, and the definition of the linear fractional transformation `lft` is according to Skogestad and Postlethwaite (2005).

We would like to ensure robust stability and robust performance. However, by the main loop theorem, it is sufficient to ensure robust performance since this implies robust stability assuming nominal stability. Since we look at robust performance, it is interesting to use D-K-iterations for the problem given in (17). The performance weights are defined as:

$$W_P = \frac{s/M + \omega_{CL}}{s + \omega_{CL} A}, \quad W_U = \frac{0.4B^2(s^2 + \sqrt{2}\omega_2 + \omega_2^2)}{s^2 + B\sqrt{2}\omega_2 s + (B\omega_2)^2}, \tag{19}$$

with ω_{CL} the desired closed-loop bandwidth, A the desired disturbance attenuation inside the bandwidth, and M the desired

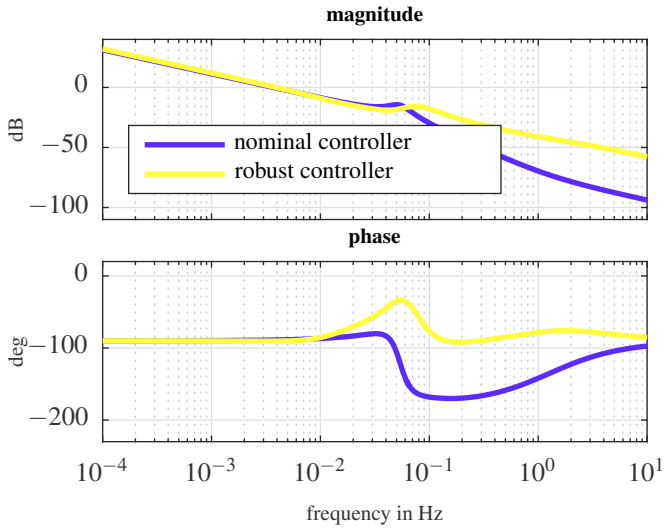

Fig. 7: Bode plot comparison between the nominal $\mathcal{H}_\infty$ controller and the robust $\mathcal{H}_\infty$ controller.

bound on $||S_p||_\infty$ and $||T_p||_\infty$. In this work, the desired closed-loop bandwidth is set to $\omega_{CL} = 0.001$ and the design bandwidth $\omega_2 = 0.02$ is chosen according to the yaw actuator limitation that is $1\,\mathrm{deg/s} \approx 0.017\,\mathrm{rad/s}$. The parameters $M = 4$, $B = 20$ and $A = 10^{-6}$ are used to shape the desired performances and $W_T = 0$.

5. RESULTS

In this section, the robust controller design results are analyzed and compared to a nominal $\mathcal{H}_\infty$ controller. Then, the controller performances are analyzed for all fifteen models. Finally, the robust controller is used in the CFD model WFSim to control the wake position under varying atmospheric inflow conditions.

5.1 Controller evaluation

A nominal $\mathcal{H}_\infty$ controller is designed like presented in Raach et al. (2016a) using the performance weights as defined in (19). The controller design achieves a controller resulting in $||N||_\infty = 0.99$. First, in Fig. 7 the Bode plot of the robust and the nominal $\mathcal{H}_\infty$ controller are shown. Clearly, the differences between the two controllers can best be seen in the high frequency region.

As a next step, the performance of both controllers is evaluated for the nominal plant. Fig. 8 shows the sensitivity S the controller sensitivity KS and the complimentary sensitivity T obtained with the nominal and the robust controller. Clearly, differences in the controller sensitivity between 10^{-2} and 10^{0} Hz are observable.

Finally, the sensitivity and the controller sensitivity are analyzed for all fifteen plants $G_l(s)$. Fig. 9 presents the results of the performance analysis of the robust $\mathcal{H}_\infty$ controller. As expected, the controller meets the desired performances for all plants $G_l(s)$.

5.2 Simulation results

The robust $\mathcal{H}_\infty$ controller is applied in the WFSim simulation model to control the wake position. To evaluate the ability to

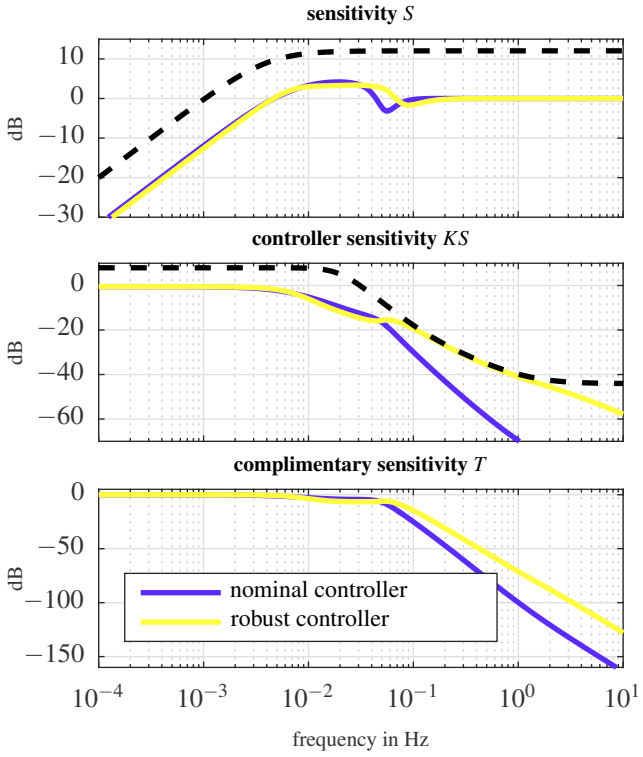

Fig. 8: Comparison between the controller performances of the nominal $\mathcal{H}_\infty$ controller and the robust $\mathcal{H}_\infty$ controller.

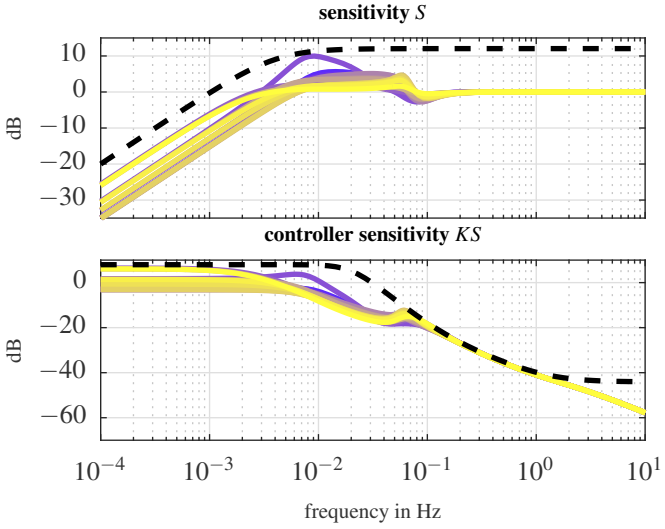

Fig. 9: Comparison of the controller performance of the $\mathcal{H}_\infty$ controller for all plants $G_l(s)$.

control the wake position under various atmospheric conditions, the inflow is continuously increased from $6\,\mathrm{m/s}$ to $10\,\mathrm{m/s}$ and exemplary set point changes are applied. See Fig. 10 for flow snapshots at different times during the simulation. Further, time series results of the estimated wake center and the input signal are given. Altogether, the controller performs well for the varying wind speeds and the desired set point changes. Only small differences in the wake center can be observed in accordance to the performance evaluation in Fig. 9.

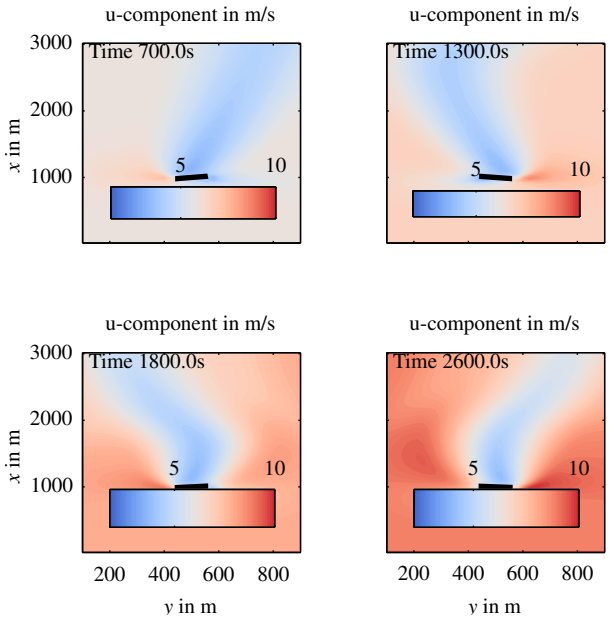

Fig. 10: Flow snapshots of the simulation with varying inflow conditions. The inflow is increased in steps from 6 m/s to 10 m/s, see Fig. 11.

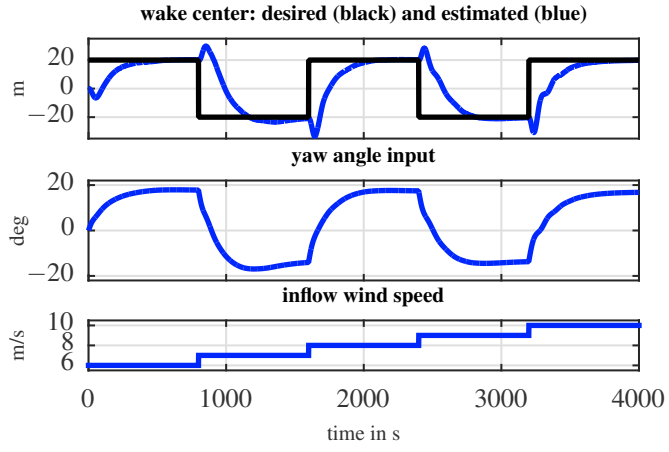

Fig. 11: The desired wake center and the estimated wake center are compared in the first time series plot. The second time series plot shows the input signal set by the $\mathcal{H}_\infty$ controller. The wind speed change is shown in the last plot.

6. CONCLUSION

In this work, a robust $\mathcal{H}_\infty$ controller design for closed-loop wake redirection was presented, including model identification, controller analysis, and simulation results. The necessity of a robust controller was shown by analyzing various step simulations with different atmospheric conditions. Further, since the measurements are not precise (uncertain), it is important to have performance under this uncertainty. An uncertain plant is derived from model identification and used in a robust $\mathcal{H}_\infty$ controller design synthesis. The closed-loop performance of the controller is analyzed and a simulation study with varying atmospheric inflow conditions is conducted in which the wake position is redirected. Altogether, the controller shows promising results.

As a next step, the approach will be combined with lidar wake tracking methods and transferred to a high-fidelity CFD model to show its applicability in complex flow situations. A controllability and observability analysis should be performed in future work. Further, the controller will be extended to also consider axial induction control.

REFERENCES

Annoni, J., Gebraad, P.M.O., Scholbrock, A.K., Fleming, P.A., and van Wingerden, J.W. (2016). Analysis of axial-induction-based wind plant control using an engineering and a high-order wind plant model. *Wind Energy*, 19(6), 1135–1150.

Boersma, S., Doekemeijer, B.M., Gebraad, P.M.O., Fleming, P.A., Annoni, J., Scholbrock, A.K., Frederik, J.A., and van Wingerden, J.W. (2017). A tutorial on control-oriented modelling and control of wind farms. In *Proceedings of the American Control Conference (ACC)*.

Boersma, S., Vali, M., Kühn, M., and van Wingerden, J.W. (2016). Quasi linear parameter varying modeling for wind farm control using the 2D Navier-Stokes equations. In *Proceedings of the American Control Conference (ACC)*.

Fleming, P., Gebraad, P., Lee, S., van Wingerden, J.W., Johnson, K., Churchfield, M., Michalakes, J., Spalart, P., and Moriarty, P. (2015). Simulation comparison of wake mitigation control strategies for a two-turbine case. *Wind Energy*, 18(12), 2135–2143.

Fleming, P.A., Gebraad, P.M., Lee, S., van Wingerden, J.W., Johnson, K., Churchfield, M., Michalakes, J., Spalart, P., and Moriarty, P. (2014). Evaluating techniques for redirecting turbine wakes using SOWFA. *Renewable Energy*, 70, 211–218.

Gebraad, P.M.O., Teeuwisse, F., van Wingerden, J.W., Fleming, P.A., Ruben, S., Marden, J., and Pao, L. (2016). Wind plant power optimization through yaw control using a parametric model for wake effects - a CFD simulation study. *Wind Energy*, 19(1), 95–114.

Jiménez, Á., Crespo, A., and Migoya, E. (2010). Application of a LES technique to characterize the wake deflection of a wind turbine in yaw. *Wind Energy*, 13(6), 559–572.

Ljung, L. (ed.) (1999). *System Identification (2Nd Ed.): Theory for the User*. Prentice Hall PTR, Upper Saddle River, NJ, USA.

Marshall, L. Buhl, J. (2005). A new empirical relationship between thrust coefficient and induction factor for the turbulent windmill state. Technical report, National Renewable Energy Laboratory.

Raach, S., Schlipf, D., Borisade, F., and Cheng, P.W. (2016a). Wake redirecting using feedback control to improve the power output of wind farms. In *Proceedings of the American Control Conference (ACC)*.

Raach, S., Schlipf, D., and Cheng, P.W. (2016b). Lidar-based wake tracking for closed-loop wind farm control. In *Journal of Physik: Conference Series, The Science of Making Torque from Wind*.

Raach, S., van Wingerden, J.W., Boersma, S., Schlipf, D., and Cheng, P.W. (2017). Hinf controller design for closed-loop wake redirection. In *Proceedings of the American Control Conference (ACC)*.

Skogestad, S. and Postlethwaite, I. (2005). *Multivariable Feedback Control: Analysis and Design*. John Wiley & Sons.